Osteoarthritis and Cartilage 27 (2019) 1481–1490

Osteoarthritis and Cartilage

T2* and quantitative susceptibility mapping in an equine model of post-traumatic osteoarthritis: assessment of mechanical and structural properties of articular cartilage

O. Nykänen † *, J.K. Sarin † ‡, J.H. Ketola † §, H. Leskinen †, N.C.R. te Moller ‖, V. Tiitu ¶, I.A.D. Mancini ‖, J. Visser #, H. Brommer ‖, P.R. van Weeren ‖, J. Malda ‖ #, J. Töyräs † ‡ ††, M.J. Nissi † §

† *Department of Applied Physics, University of Eastern Finland, Kuopio, Finland*
‡ *Diagnostic Imaging Center, Kuopio University Hospital, Kuopio, Finland*
§ *Research Unit of Medical Imaging, Physics and Technology, University of Oulu, Oulu, Finland*
‖ *Department of Equine Sciences, Faculty of Veterinary Medicine, Utrecht University, Utrecht, The Netherlands*
¶ *Institute of Biomedicine, Anatomy, University of Eastern Finland, Kuopio, Finland*
# *Department of Orthopaedics, University Medical Center Utrecht, Utrecht, The Netherlands*
†† *School of Information Technology and Electrical Engineering, The University of Queensland, Brisbane, Australia*

ARTICLE INFO

Article history:
Received 8 February 2019
Accepted 25 June 2019

Keywords:
Articular cartilage
Quantitative susceptibility mapping
T2* relaxation
Post-traumatic osteoarthritis

SUMMARY

Objective: To investigate the potential of quantitative susceptibility mapping (QSM) and T2* relaxation time mapping to determine mechanical and structural properties of articular cartilage via univariate and multivariate analysis.

Methods: Samples were obtained from a cartilage repair study, in which surgically induced full-thickness chondral defects in the stifle joints of seven Shetland ponies caused post-traumatic osteoarthritis (14 samples). Control samples were collected from non-operated joints of three animals (6 samples). Magnetic resonance imaging (MRI) was performed at 9.4 T, using a 3-D multi-echo gradient echo sequence. Biomechanical testing, digital densitometry (DD) and polarized light microscopy (PLM) were utilized as reference methods. To compare MRI parameters with reference parameters (equilibrium and dynamic moduli, proteoglycan content, collagen fiber angle and -anisotropy), depth-wise profiles of MRI parameters were acquired at the biomechanical testing locations. Partial least squares regression (PLSR) and Spearman's rank correlation were utilized in data analysis.

Results: PLSR indicated a moderate-to-strong correlation (ρ = 0.49–0.66) and a moderate correlation (ρ = 0.41–0.55) between the reference values and T2* relaxation time and QSM profiles, respectively (excluding superficial-only results). PLSR correlations were noticeably higher than direct correlations between bulk MRI and reference parameters. 3-D parametric surface maps revealed spatial variations in the MRI parameters between experimental and control groups.

Conclusion: Quantitative parameters from 3-D multi-echo gradient echo MRI can be utilized to predict the properties of articular cartilage. With PLSR, especially the T2* relaxation time profile appeared to correlate with the properties of cartilage. Furthermore, the results suggest that degeneration affects the QSM-contrast in the cartilage. However, this change in contrast is not easy to quantify.

* Address correspondence and reprint requests to: O. Nykänen, Department of Applied Physics, University of Eastern Finland, POB 1627, FI-70211, Kuopio, Finland.
E-mail addresses: olli.nykanen@uef.fi (O. Nykänen), jaakko.sarin@uef.fi (J.K. Sarin), juuso.ketola@oulu.fi (J.H. Ketola), henriles@uef.fi (H. Leskinen), N.C.R.teMoller@uu.nl (N.C.R. te Moller), virpi.tiitu@uef.fi (V. Tiitu), I.A.D.Mancini@uu.nl (I.A.D. Mancini), jetzevisser.jv@gmail.com (J. Visser), H.Brommer@uu.nl (H. Brommer), r.vanweeren@uu.nl (P.R. van Weeren), J.Malda@umcutrecht.nl (J. Malda), j.toyras@uq.edu.au (J. Töyräs), mikko.nissi@uef.fi (M.J. Nissi).

https://doi.org/10.1016/j.joca.2019.06.009

Introduction

Osteoarthritis (OA) is a progressive disease that leads to restricted mobility and severe joint pain[1,2]. The onset of OA may be due to joint trauma, such as a ligamental tear or focal cartilage loss.[2] Magnetic resonance imaging (MRI) is among the best non-invasive tools available for diagnosis of OA. Especially, quantitative MRI methods have been proposed for diagnosis of OA.[3] However, quantitative parameters are usually time-consuming to measure in full 3-D imaging due to the requirement of multiple datasets to allow for data quantification (e.g., measurement of T1 relaxation time using gold standard inversion recovery sequence); furthermore, they usually require specific sequence design.[4–7]

To overcome the limitations set by desired imaging time and resolution, we propose the use of quantitative susceptibility and T2* relaxation time mapping (QSM and T2*, respectively) that are measurable using standard multi-echo gradient echo sequences. QSM maps the magnetic susceptibility distribution inside the imaging target, which can be altered for example by accumulation of iron or calcifications inside the target region.[8–11] In OA, mineralization of cartilage has been reported[12,13]; hence QSM might be sensitive in diagnosis of OA. So far, mostly preliminary studies with limited data sets on QSM of articular cartilage have been reported.[14–16] Wei *et al.* showed that susceptibility of articular cartilage displays orientational anisotropy and that the susceptibility has depth-wise varying contrast in articular cartilage.[14] In another study, Wei *et al.* utilized the anisotropy of susceptibility to perform collagen fiber orientation tracking using susceptibility tensor imaging.[15,17] Nykänen *et al.* showed that proteoglycan loss did not affect the susceptibility in *ex vivo* cartilage.[16] The same study also revealed that anisotropy of QSM was seemingly different from the anisotropy of T2* relaxation, which has been linked to the structural anisotropy of the collagen network in cartilage.[16,18] Furthermore, in a recent *in vivo* study, Wei *et al.* have shown that the decrease of depth-wise variation in the susceptibility is linked to osteoarthritis *in vivo*.[19]

In conclusion, previous studies have pointed out that the collagen fiber orientation could be the source of the QSM contrast in the cartilage. Besides the few studies on articular cartilage, some QSM studies have targeted the venous structures of the epiphyseal-articular cartilage complex.[20–23] T2* and related T2 relaxation time measurements have been studied more extensively in cartilage imaging and have been related to properties of the collagen network.[24] Our aim was to validate the use of QSM and T2* for prediction of cartilage biomechanical and structural properties using samples from an equine post-traumatic OA study.[25] We hypothesized (1) that cartilage properties can be predicted from depth-wise profiles of quantitative MRI-parameters using partial least squares regression (PLSR) and (2) that this is a more sophisticated way of utilizing MRI data than direct Spearman's rank correlation analysis between bulk values of quantitative MRI and reference parameters.

Methods

Samples

Osteochondral samples were obtained from a cartilage repair study involving seven Shetland ponies ($N = 7$, 6 females and 1 male, Age = 8.8 ± 3.5 years).[25] For the repair study, surgical lesions were induced in the medial trochlear cartilage in both hinds and repaired with a combination of chondrons and mesenchymal stem cells in different carrier hydrogels. The ponies were sacrificed after 1 year. Wedge-shaped samples (Fig. 1) were collected from the medial trochleae post-mortem and included part of the lesions as well as surrounding cartilage. Stifle joints from three healthy ponies (with matching age range) were acquired from a local abattoir (van de Veen, Nijkerk, The Netherlands). From these stifles six control samples (one from each stifle) were taken, leading to a total of 20 samples (14 experimental, 6 control). The number of animals was based on the power calculations performed for the original cartilage repair study.[26]

The ethical permission for animal study was given by the Ethics Committee of Utrecht University for Animal Experiments in compliance with the Institutional Guidelines on the Use of Laboratory Animals. The animal study was carried out in a surgical theatre at the Department of Equine Sciences, Utrecht University, The Netherlands (Permission DEC 2014.III.11.098).

Biomechanical testing, digital densitometry, and polarized light microscopy

Prior to MRI, the samples underwent biomechanical indentation testing. The indentation was performed using a system that had a 250 g load cell (accuracy ± 0.25%, Model 31, Honeywell Sensotec Sensors, Columbus, OH, USA) and an actuator (displacement resolution 0.1 μm, PM500-1 A, Newport, Irvine, CA, USA). Several locations (proximal, central and distal with respect to the anatomical location in the joint) were investigated, because cartilage thickness and properties vary throughout the joint. Thus, biomechanical measurements were conducted on a pre-defined grid of 12 testing locations on each sample (Fig. 1), leading to a total number of 235 biomechanical testing locations (two samples had less than 12 locations).[25] Adjacent points could be measured after each other in quick succession since the utilized indender had a small diameter (~0.5 mm) compared to the distance between the adjacent points (~3–4 mm).[27] Equilibrium and dynamic moduli were determined from the biomechanical testing results.

After the MRI measurements, the samples were fixed in formalin and then decalcified in EDTA to soften them for histological sectioning. Sections were cut to include two biomechanical testing locations with matching distances from the edges of the block to ensure reliable location matching for microscopical imaging. Sections were stained using safranin-O for digital densitometry (DD) analysis to reveal proteoglycan content.[28] The staining was done in one process, using the same batch of dye for all the slices to ensure consistency of the stain concentration. Unstained sections were digested with hyaluronidase to remove proteoglycans to prepare them for polarized light microscopy (PLM), which was used to reveal collagen fiber angles and anisotropy.[29]

DD was performed using a light microscope equipped with a monochromatic light source and a CCD-camera. The settings of the microscope and the camera were the following: objective 1×, zoom 2×, binning 1 and calibration with neutral density filters of 0–3.0 optical density. The optical density of each sample was calculated based on the calibration set. To calculate the average depth-dependent profile for each measurement location, the subchondral bone was manually segmented from the images, followed by automatic extraction of profiles perpendicular to the cartilage surface and interpolation of profiles to 100 points. The analysis was performed with a custom Matlab algorithm (Matlab 2016b, Mathworks, Inc.).

PLM was performed using an Abrio PLM imaging system (CRi Inc., Woburn, MA, USA) which was mounted on a light microscope (Nikon Diaphot TMD, Nikon Inc., Shinagawa, Tokyo, Japan). The pixel size for both PLM and DD images was 3.5 μm × 3.5 μm. The fiber angle anisotropy was calculated from fiber angle images using the following equation:

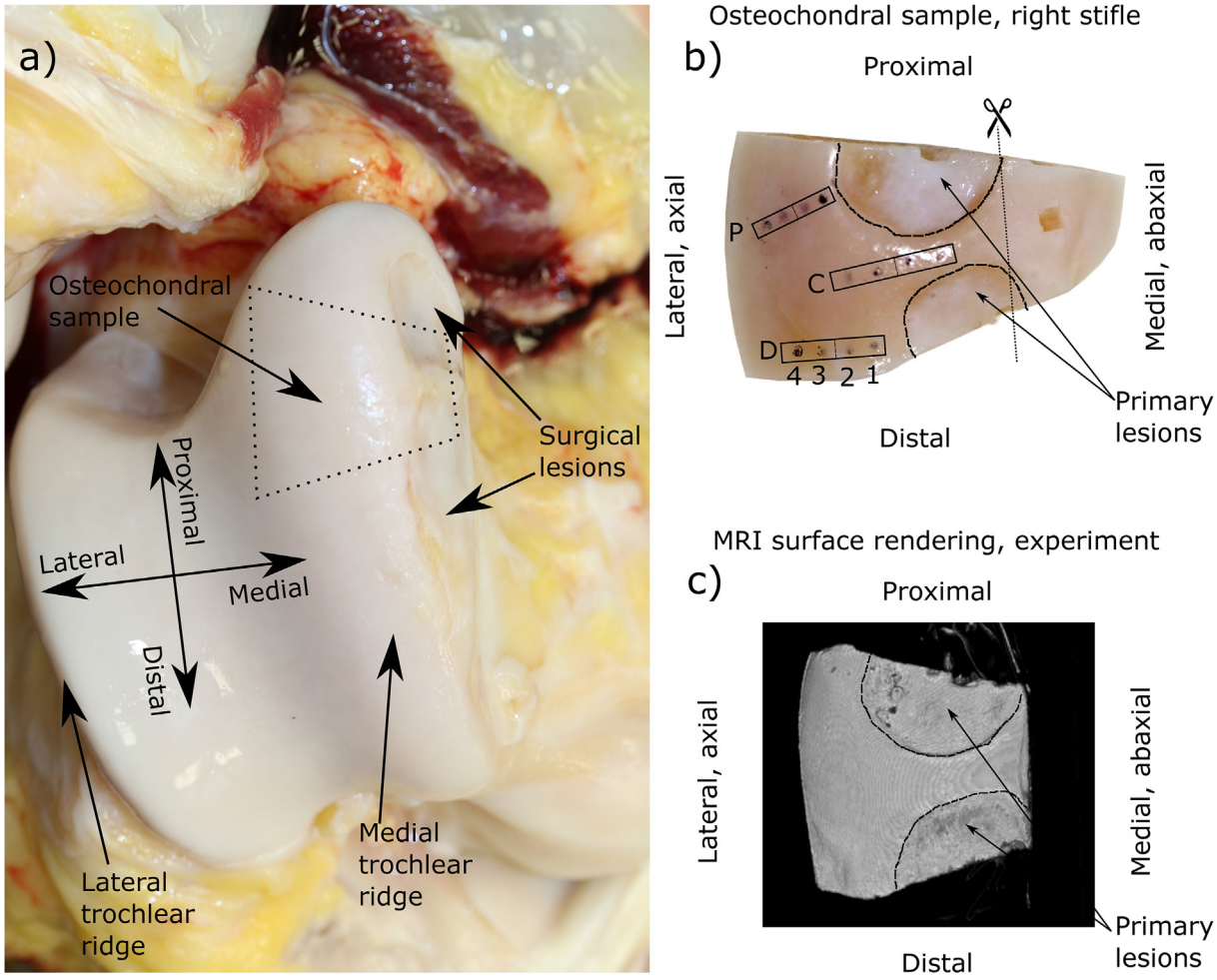

Fig. 1. a) Anterior-posterior view of right trochlea of an experimental animal, b) photograph of an experimental sample and c) a corresponding surface rendering of a 3-D MR image. The surgically-induced lesions are highlighted with dashed lines and light black dots indicate the biomechanical testing points. The boxes indicate the areas where histological slices were cut. The line with scissors indicates where the sample blocks were trimmed to fit them into the MRI coil. Letters P, C, D (proximal, central, distal) and numbers from 1 to 4 indicate the naming of the individual measurement points, e.g., P4 is the proximal point furthest away from the lesion. Distal and lateral aspects are towards the weight bearing regions in the stifle joint.

$$A_{\mathrm{PLM}}(r) = \frac{1}{1+\varepsilon(r)}. \quad (1)$$

where $\varepsilon(r)$ is the pixel-wise local entropy of a 5-by-5 pixel region in the collagen fiber orientation image. This method was used since it provides a good approximation of the true collagen fiber anisotropy[29], which could not be calculated directly due to lack of access to the raw data acquired with the Abrio system. The fiber angle and anisotropy profiles were gathered from microscope images using a similar procedure as in optical density measurements.

MRI

MRI was performed in a 9.4 T vertical bore small animal scanner using a 19-mm-diameter quadrature RF volume transceiver (Rapid Biomedical, Rimpar, Germany). The samples were immersed in 1HMRI-signal-free perfluoropolyether oil (Galden HS 240, Solvay Solexis, Brussels, Belgium) inside a thin latex holder. During MRI, the cartilage surface was oriented approximately perpendicular to the main magnetic field of the scanner with extreme care, as orientation-anisotropy has been reported for both T2* and QSM of articular cartilage.[15,16,18] Imaging was conducted using a multi-echo gradient echo sequence with six echoes. The first echo time of the sequence was 2.0 ms and echo spacing was 3.05 ms. Isotropic voxel size of 100 × 100 × 100 μm^3 was used and the matrix size of the image was 200 × 256 × 200 voxels. The longest dimension, which was also the readout direction, was in line with the main magnetic field of the scanner.

After collecting the raw MRI data, the T2* relaxation time as well as QS-maps were reconstructed. In QSM post-processing, the "complex fitting"−method was used to combine multi-echo data[30], followed by Laplacian unwrapping to resolve residual wraps in echo combination data.[31] The unwrapped field map was then masked using cartilage segmentation. The susceptibility maps were calculated from masked unwrapped phase data using a total field inversion (TFI) method to limit the need of region of interest (ROI) erosion in the QSM dipole inversion.[32] The erosion of the ROI in conventional QSM methods such as projection onto dipole fields (PDF) + morphology enabled dipole inversion (MEDI)[33] is depicted in supplemental material (Supplementary Fig. S1). The susceptibility values were referenced by setting the mean over an individual sample to zero susceptibility. T2* relaxation time maps were calculated using 2-parameter linearized fitting of the data. In the T2* fitting procedure, voxels with T2* higher than 150 ms were considered erroneous and their T2* value was set to 150 ms. Three-

dimensional surface maps were gathered from MRI parameters to visualize differences between the experimental and control samples.

Data analysis

Depth-wise profiles from the 3-D T2*- and QS- maps were obtained using cylindrical 3-D ROIs of 1-mm diameter and carefully matched with the biomechanical testing points based on μCT measurements and photographs of the samples.[25] Prior to the analysis, these profiles were interpolated into 100 depth-wise points. The profiles were then used to predict reference variables (i.e., equilibrium and dynamic moduli, proteoglycan content, collagen fiber angle and collagen anisotropy) using PLSR. Prior to the PLSR-analysis, depth profiles were normalized using standard normal variate. To avoid overfitting of the models, PLSR-analysis was conducted using 10-fold cross-validation. PLSR analysis was performed using a custom-made algorithm in MATLAB. Predictions from PLSR-analysis were compared with reference parameter values using Spearman's rank correlation analysis. In addition to PLSR-analysis, direct correlations were calculated between means of full and superficial (25% depth) MRI profiles and reference parameter values. For QSM, the range of the susceptibility values within the profile was used instead of the mean due to lack of absolute QSM referencing in the imaging.

Statistical significance of differences in tissue properties between experimental and control groups was tested with the Mann–Whitney *U* test in SPSS (Version 25, SPSS Inc., IBM Company, Armonk, NY, USA). Statistical significance of Spearman correlations was tested using exact permutation distributions in MATLAB. In both tests $P < 0.05$ was considered as the limit for statistical significance. Non-parametric tests were utilized in this study due to the non-normality of the reference data (Shapiro–Wilk test $P < 0.0001$).

Surface map analysis was conducted through the following steps. First, a tetrahedral grid was created in the cartilage mask (every 20th point of the mask was used as nodes). Surface triangles were then sought and their surface normals were calculated. After this, the 3-D QSM and T2* maps were sampled from within the volume along the surface normals. From these sampled profiles, the range for QSM and mean for T2* was calculated. Finally, the QSM range and T2* mean values were displayed on the surface triangles of the mesh to generate the parametric surface maps.

Data availability

All raw data and documentation, as well as key analysis codes used in this study, are available for download at Zenodo (https://doi.org/10.5281/zenodo.2558172).

Results

Biomechanical testing and histological analysis

Differences between experimental and control specimens were noted with all reference methods (Figs. 2–4). In biomechanical testing, both equilibrium and dynamic moduli were decreased in the experimental specimens compared to moduli of control samples at the same location ($P < 0.05$, for all distal and most of the central locations) and the differences became clearer when moving towards more distal aspect of the specimens (referring to the position in the joint) (Fig. 2). It is also worth noting that when moving towards the lesion sites (i.e., towards the medial aspect of the femoral groove), also the moduli of the control specimens decreased (Fig. 2) (see Fig. 1 for terminology). Further results of the biomechanical testing have been reported in a previous study.[25]

Overall, lower proteoglycan contents were observed in experimental specimens compared to controls. The difference between control and experimental groups was largest at the regions nearby the lesions and decreased further away from the lesions for proximal and distal locations (Figs. 3 and 4). Conversely, for central locations differences in PG content became clearer while moving away from the lesions. The collagen fiber angles in the radial zone of the experimental group were lower than in the control group and the difference between groups was highest at the locations nearby the lesions (Figs. 3 and 4), except for the proximal regions, for which no significant differences in fiber angle were observed. There were also differences between the collagen fiber anisotropy of the experimental and control groups, but contrary to the optical density and fiber angle, the differences became clearer when moving away from the lesion site and notable changes were only observed on the distal side of the specimens (Figs. 3 and 4).

MRI

QSM exhibited differences between the control and experimental groups especially nearby the lesion site in the central locations and further away from the lesion site at proximal and distal locations (Figs. 5–7). Nearby the lesion at central locations, QSM profiles had a smaller range in the experimental samples when compared to the controls (Fig. 5). When moving further away from the lesion site at distal and proximal locations, the range of the profiles increased in experimental samples when compared to the control samples (Fig. 5). Overall, QSM seemed to have more spatial variation in the experimental samples (Fig. 7).

The T2* profiles had qualitatively slightly lower maximum values nearby the lesion and higher values further away from the lesion site (Fig. 5). However, the mean value of T2* was increased nearby the lesion sites (i.e., towards the abaxial aspect of the femoral groove) in both experimental and control groups but slightly more so in the experimental specimens (Fig. 7). Cartilage thickness seemed to have no appreciable effect on the T2* or QSM values (Fig. 7, Supplementary Figs. S2–4).

Correlation and PLSR analysis

The absolute value of Spearman's rank correlation between MRI and reference parameters was between $\rho = 0.03$ and $\rho = 0.46$, with the highest correlations observed between bulk T2* and collagen anisotropy ($\rho = -0.46$) and between superficial QSM and bulk fiber angle ($\rho = 0.40$) (Table I). In general, the T2* bulk value had a stronger correlation with the reference parameters, whereas for QSM the strongest correlations were observed between the superficial QSM and the reference parameters (Table I). Most of the correlations in the direct correlation analysis were statistically significant, and only correlations near $\rho = 0.00$ were non-significant.

PLSR-modelling results showed that the estimation of the reference parameters from MRI data was more successful using T2* or a combination of T2* and QSM (apart from the superficial collagen fiber angle and anisotropy, the correlations were between $\rho = 0.49$ and $\rho = 0.68$), and less successful using QSM results only (correlations between $\rho = 0.41$ and $\rho = 0.55$) (Table I, Supplementary Fig. S5). For combined T2* and QSM, mean PLM anisotropy showed the highest ($\rho = 0.68$) and mean superficial PLM anisotropy showed the lowest ($\rho = 0.18$) correlation between predicted and measured values (Table I). All correlations from PLSR-analysis were statistically significant.

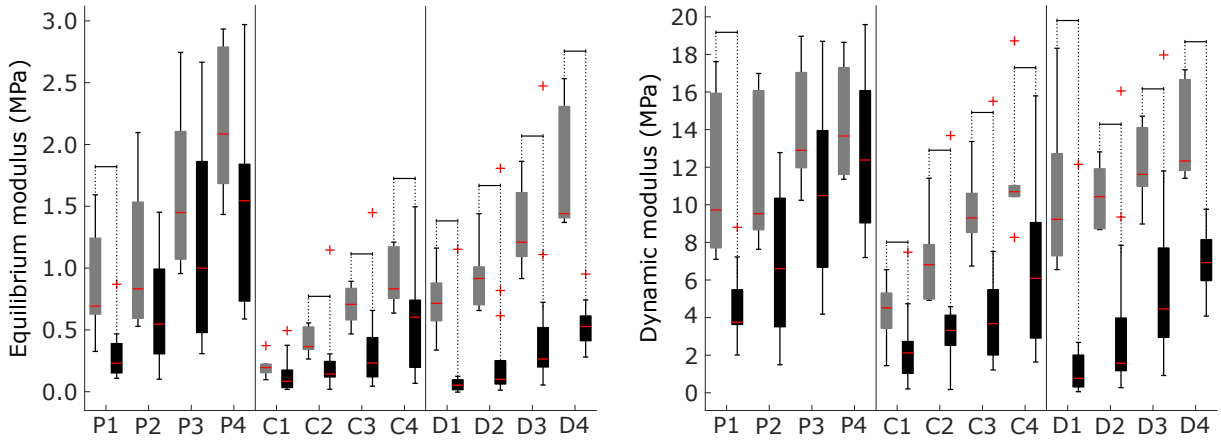

Fig. 2. Boxplots of the biomechanical properties of the samples at each of 12 measurement locations. Gray bars indicate control sample results and black bars are experimental samples. Red lines are the median values of measurements and red crosses are outliers from 25 to 75 percentile range. Brackets indicate significant ($P < 0.05$) differences between control and experimental groups.

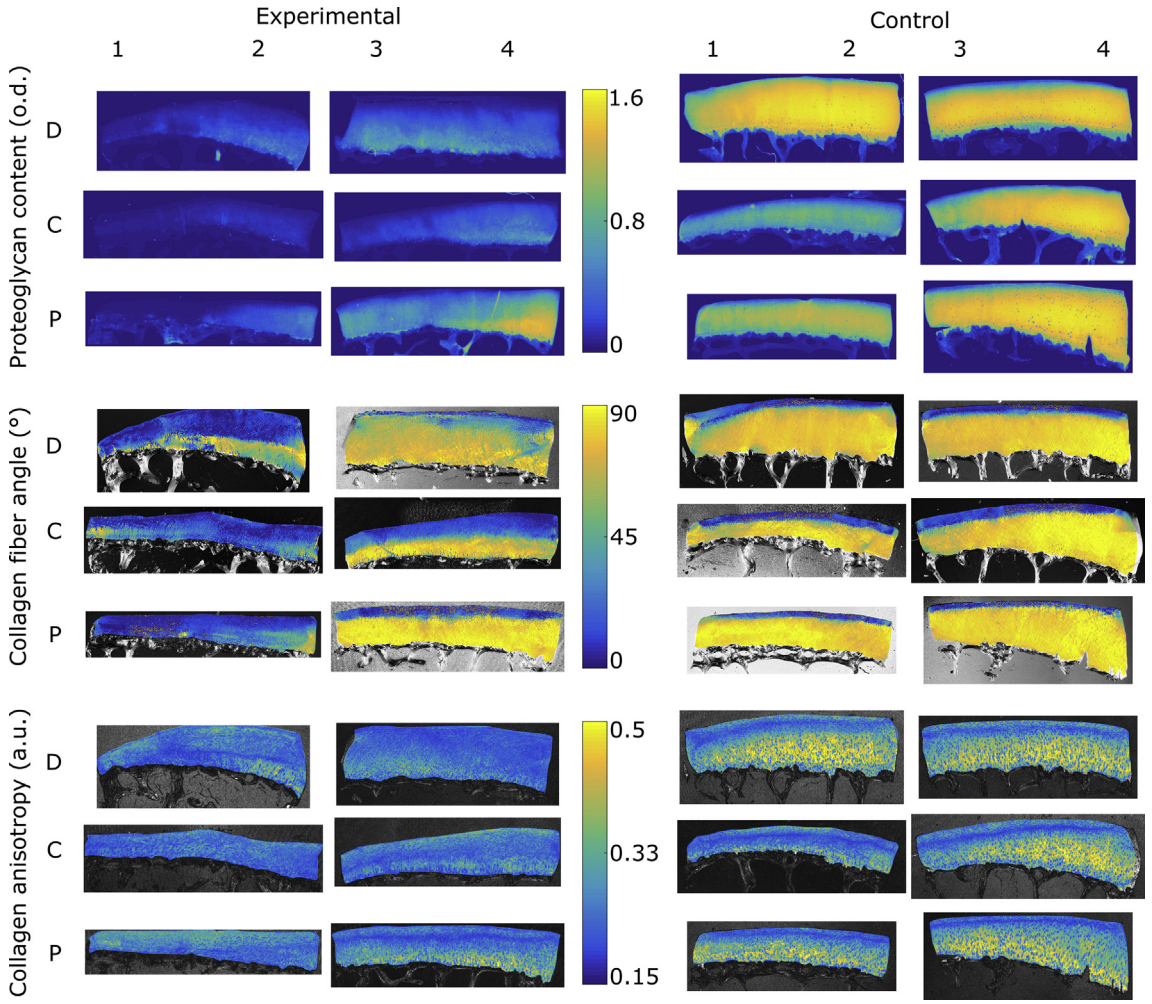

Fig. 3. Representative quantitative microscopic images (PLM fiber angle, PLM anisotropy and PG content as represented by the optical density of the safranin-O stained sections) from all measurement locations for both experimental and control samples (see Fig. 1 for histology sampling locations).

Discussion and conclusions

In this study, we examined the potential of 3-D quantitative MRI to detect post-traumatic OA (PTOA) changes in cartilage properties. More specifically, QSM and T2* relaxation time mapping were investigated and correlated with biomechanical parameters, proteoglycan content and collagen network properties. The analysis revealed weak-to-moderate direct correlations

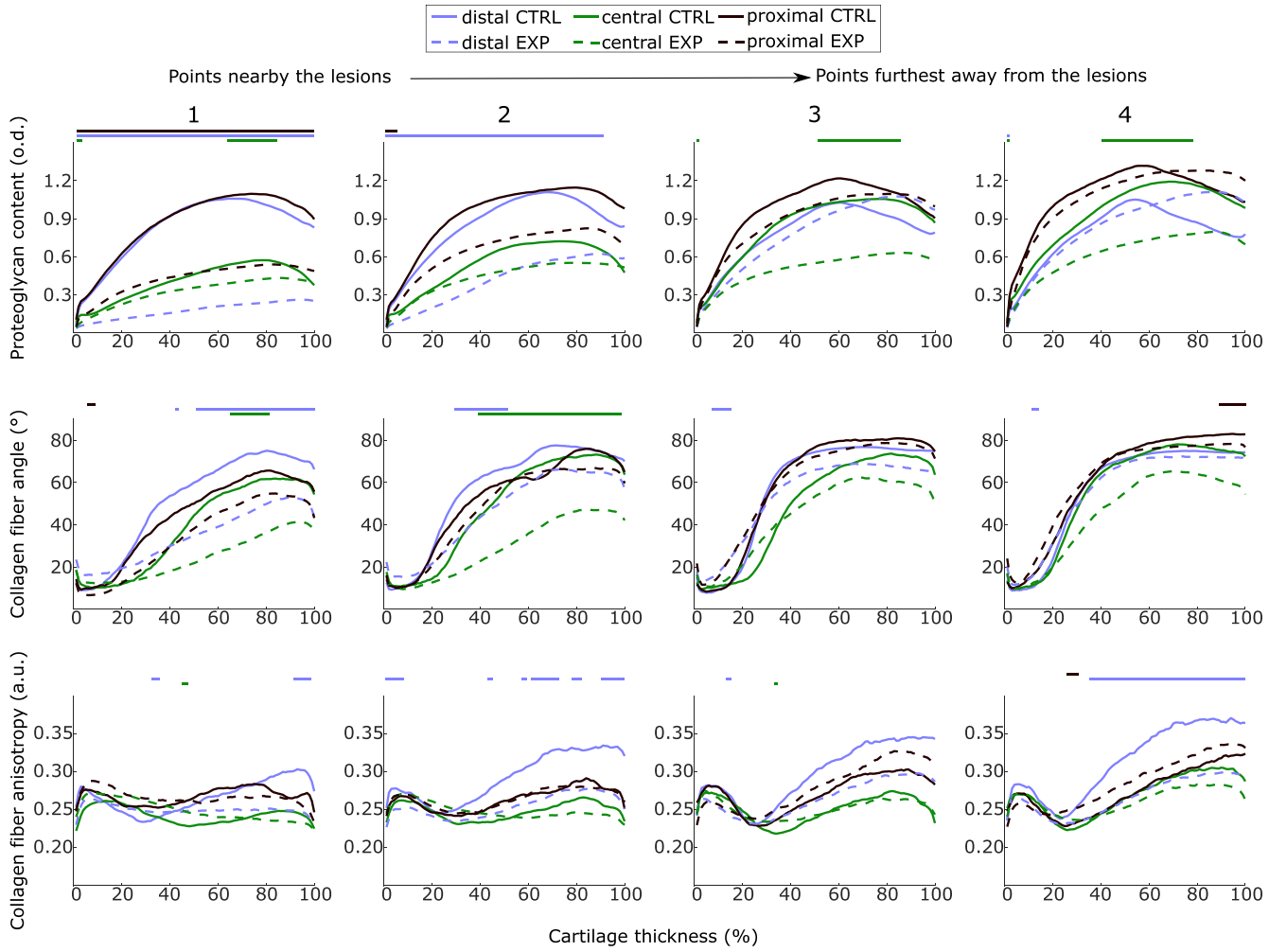

Fig. 4. Measured proteoglycan content, collagen fiber angle, and collagen anisotropy profiles of the samples at different distances from the lesion area. Profiles in the left column are from measurement points nearest to the lesions and the right column depicts the profiles from the most distant points. Solid lines depict profiles from control samples and dashed lines from experimental samples. Brown lines are from the most proximal part of the samples, green lines from the middle and bluish lines are the most distal ones (See also Fig. 1 for sampling locations). Lines at the top of the image indicate regions where the difference between control and experimental groups is statistically significant ($P < 0.05$, Mann–Whitney *U*-test).

between MRI and reference parameters. PLSR-modelling of depth-wise MRI profiles increased the correlations between MRI and reference parameters, demonstrating that PLSR outperforms univariate analysis in quantitative MRI evaluation of articular cartilage.

Especially biomechanical testing, but also quantitative microscopic analyses (DD and PLM) revealed differences between the experimental and control samples (Figs. 2–4). Interestingly, large intrasample differences in both DD and PLM were observed within both experimental and control groups (Figs. 2–4). This could indicate that the cartilage nearby the trochlear ridges of femur is different from the cartilage in more central locations of the knee joint (Figs. 2–4). Particularly interesting were the PLM results, showing that the cartilage seemed to lose its usual trilaminar appearance nearby the lesion sites in both experimental and control groups and instead had fibers directed parallel to the cartilage surface throughout the cartilage thickness (Figs. 3 and 4). Marked structural changes in the properties of the collagen fiber network have been demonstrated earlier at the edges of canine humeral cartilage.[34]

T2* relaxation time mapping was done using linear fitting through magnitude images of each individual echo of multi-echo gradient echo sequences. This procedure is well-established in cartilage MRI. T2*-mapping revealed the usual trilaminar appearance in both experimental and control groups further away from the trochlear ridge (Fig. 6). However, at locations nearby the ridge or lesion site, this trilaminar appearance was less visible, especially in the experimental group (Fig. 6). This supports the idea that cartilage near the lesion area exhibits degenerative changes. It is worth noting that for T2* results, the same main relaxation contributions should apply as for the more commonly used T2 relaxation time, because cartilage does not contain high susceptibility differences or other field homogeneity issues that would differentiate T2* from T2.

Both T2* and QSM displayed visual differences between the experimental and control samples (Figs. 5–7, Supplementary Figs. S1–3). The surface visualization revealed more distinct changes in QS- than in T2*-maps. However, these changes were difficult to quantify, which may be reflected in the poorer PLSR-modelling results. One notable feature in QSM was the flattening of QSM depth profiles at central measurement points in the experimental group when compared to the control samples. This finding is in line with a recent study, statingtural that depth-wise standard deviation of QSM is decreased in OA.[19] The direct

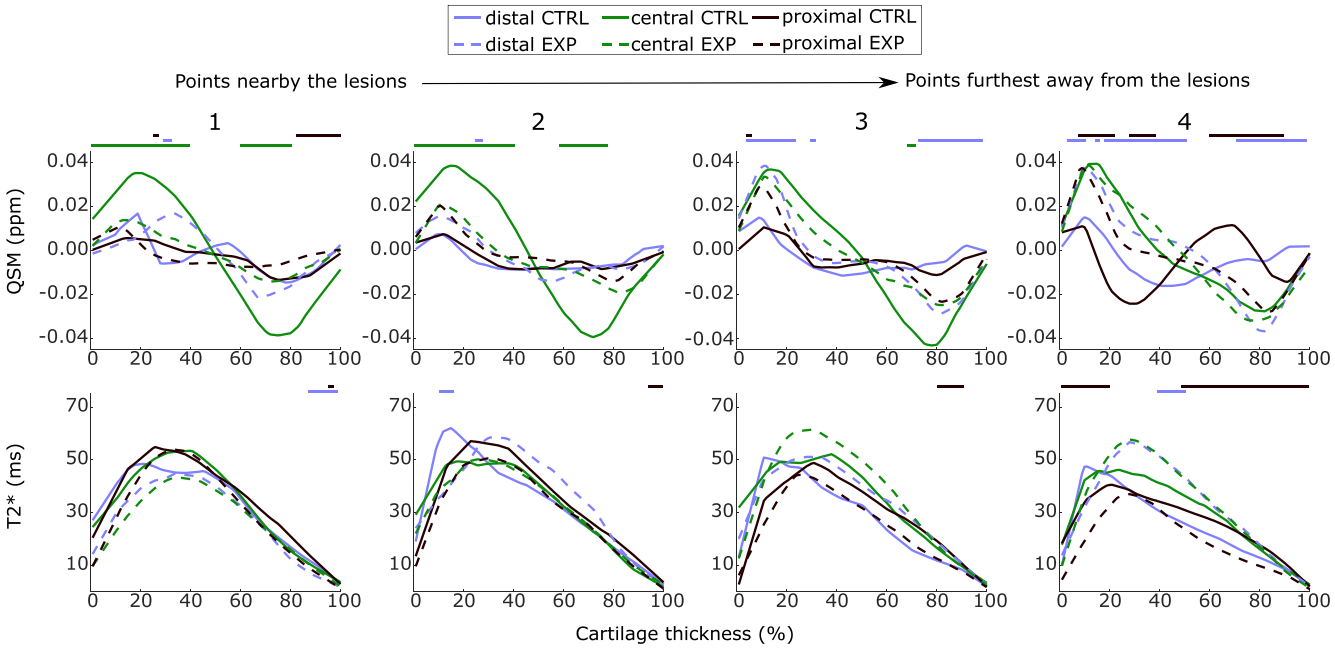

Fig. 5. Measured QSM and T2* depth profiles of the samples moving away from the lesion area. Left column contains profiles from the measurement points nearest to the lesions and the right column contains profiles from the most distant points. Solid lines depict profiles from control samples and dashed lines from experiment samples. Brown lines are from the most proximal part of the samples, green lines from the middle and bluish lines are the most distal ones (See also Fig. 1 for sampling locations). Lines at the top of the image indicate regions, where the difference between control and experimental groups is statistically significant ($P < 0.05$, Mann–Whitney *U*-test).

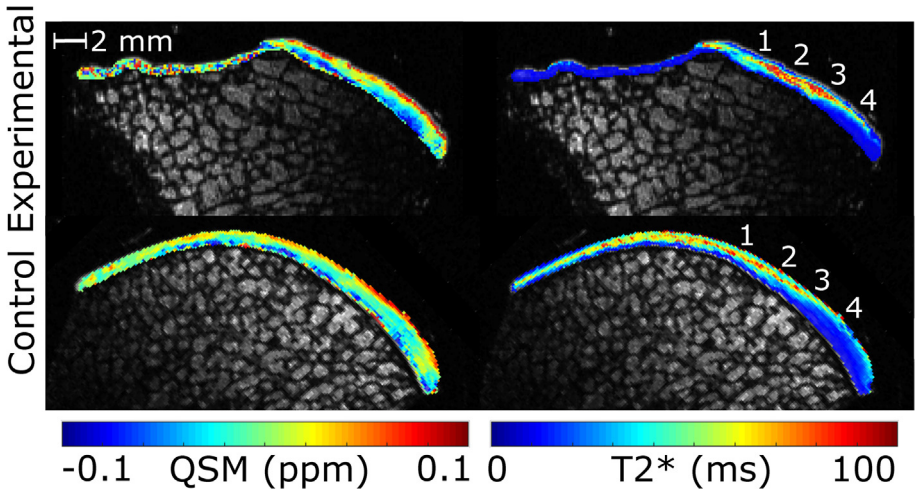

Fig. 6. Representative QS- and T2*-maps for experimental and control samples. Parameter maps are overlaid on magnitude images from MRI. Numbers 1–4 indicate the approximate locations of the biomechanical testing sites.

correlations between T2* and biomechanical and structural properties of cartilage were similar to those that have previously been reported between T2 and cartilage properties.[35,36] Furthermore, the PLSR-modelling yielded higher correlations between MRI and other cartilage properties than direct univariate analysis. Thus, in the future, modelling approaches such as artificial neural networks and PLSR would be preferred in the analysis of quantitative MRI of cartilage. While the PLSR-modelling could have certainly benefitted from an even larger data set, it outperformed direct correlation ($\rho_{bulk} = 0–0.46$) already in this limited data set and yielded high correlations ($\rho_{PLS} = 0.41–0.68$) between the predicted and measured reference parameters in analyses which took full-depth profiles into account.

In this study, QSM-post processing was based on the "complex fitting", Laplacian unwrapping and Total Field Inversion steps.[30–32] Several studies have been dedicated to finding the most appropriate processing pathways and methods, especially for brain imaging, which has been the main target for QSM.[9,37] For cartilage, QSM has not been fully established for imaging small *ex vivo* cartilage specimens, a concern that was also raised in a previous study.[16] The fundamental difficulty in QSM imaging of small *ex vivo* cartilage samples is that regardless of the methodology, the accuracy of QSM is sub-optimal nearby the boundaries of the ROI.[38,39] Due to the thinness of cartilage, the entire ROI comprising cartilage is always near to a tissue boundary, making QSM difficult. Here we utilized TFI because it doesn't necessitate erosion of the already-thin cartilage mask. Supplementary material (Supplementary Fig. S1) provides a brief comparison of different methods and the implications with respect to small ROI. Encouragingly however, differences between the experimental and control groups were

Table I
Spearman rank correlations between MRI and reference parameters. In parentheses, normalized root mean square errors (%) for PLSR-predictions are presented. See Supplementary Fig. 4 for scatter plots of PLSR-modelling. Entries marked with * are statistically significant ($P < 0.05$)

	Spearman correlations between MRI values and reference parameters							
	Equilibrium modulus	Dynamic modulus	Proteoglycan content	Superficial PG content	Collagen fiber angle	Superficial fiber angle	Collagen fiber anisotropy	Superficial anisotropy
QSM	0.07	0.07	0.15*	0.16*	0.24*	0.24*	0.03	−0.22*
T2*	−0.35*	−0.33*	−0.26*	−0.23*	−0.30*	−0.19*	−0.46*	−0.08
Superficial QSM	0.29*	0.26*	0.34*	0.34*	0.40*	0.32*	0.26*	−0.16*
Superficial T2*	−0.08	−0.08	−0.10	−0.05	−0.06	−0.06	−0.10	−0.03
	Spearman correlations and NRMSE between PLS predictions and reference parameters							
QSM + T2*	0.61* (15.95)	0.61* (20.10)	0.67* (20.02)	0.67* (18.08)	0.61* (20.84)	0.41* (16.76)	0.68* (16.04)	0.23* (18.11)
QSM	0.47* (17.80)	0.41* (23.16)	0.55* (23.24)	0.51* (20.74)	0.44* (22.89)	0.32* (17.34)	0.47* (19.60)	0.21* (17.82)
T2*	0.56* (18.05)	0.52* (21.74)	0.66* (22.67)	0.57* (20.12)	0.49* (22.65)	0.34* (17.44)	0.63* (16.87)	0.18* (18.43)

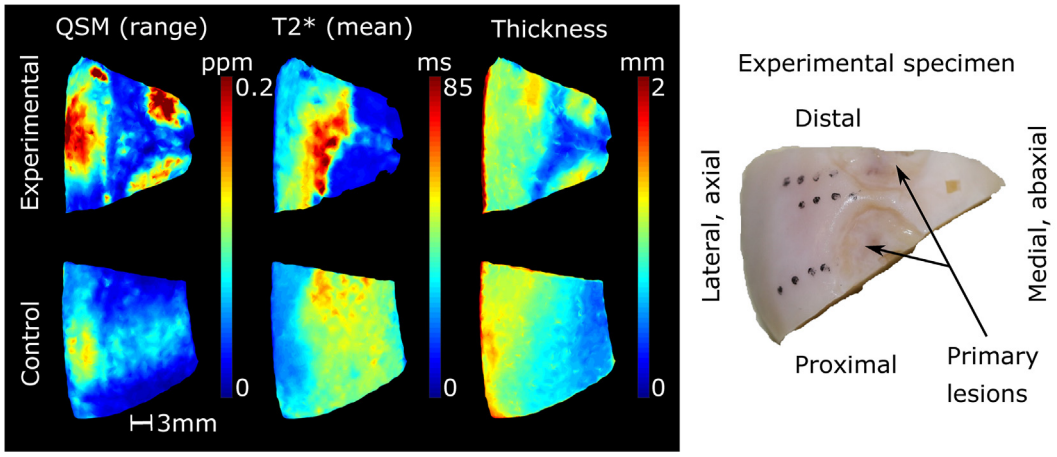

Fig. 7. 3-D surface visualization of the QSM range, mean T2*, and cartilage thickness throughout the specimen. Top row experimental samples, bottom control samples. The photograph on the right provides visual comparison of the lesions and reference measurement points. The images are approximately in the same geometric scale, and the orientation is approximately the same for the experimental and control samples. Please note also that part of the sample was trimmed before MRI (See also Fig. 1). For surface maps of the entire data set, see Supplementary Figs. 1–3 Please note that the scale for QSM is from 0.0 to 0.2 ppm since the range (through the cartilage thickness) always has a positive value.

detected in this study even though the processing is not fully optimized for such thin tissue structures of interest. *In vivo* imaging should at least partially overcome this problem, as there will be lots of other nearby signal sources in addition to cartilage, improving the susceptibility processing. Another fundamental difficulty (or perhaps a property) with the current QSM processing methods is that the susceptibility values are relative to the imaged target, i.e., if susceptibility is increased by 0.05 ppm in the whole target, this change may not be detectable. Thus referencing (e.g., adding a capsule of oil near the target tissue) would be beneficial in the QSM studies of cartilage or of any other tissue.[9,37]

The main limitation of this study is the lack of referencing in QSM reconstructions, which was partially dealt with by using the range instead of the mean in the direct analysis. QSM could also have benefitted from imaging in signal-producing media such as saline instead of signal-free perfluoropolyether. On the other hand, this would have led to lower resolution due to potential wrapping in the phase encoding direction. Furthermore, the measurement of the T2* relaxation time may have been suboptimal since the last echo time (17.25 ms) was considerably shorter than the longest measured T2* relaxation times (~70 ms). However, this is considered to have only a small effect on the analysis of the data, since two-parameter linear fitting of T2* relaxation time is a relatively robust method. The robustness of the fit was further enhanced by limiting the maximum allowed value of T2* to 150 ms, which is a sufficient limit for the T2* of articular cartilage. The sequence parameters were optimized for QSM measurement, relieving the strain on the gradient system by reducing the number of echoes; the longest echo times were limited, thus briefly compromising the accuracy of the T2* relaxation time mapping. For PLSR-analysis, the dataset could have been larger, since intrasample differences were higher than expected (especially for PLM), which may affect the PLSR results due to the relatively high number of potential outliers in the data. While the number of animals as such may be considered low for the PLSR-analysis, the limitation was mitigated by performing multiple measurements at different locations in each sample, leading to a sufficiently high number of data points for the analysis. Furthermore, other qMRI parameters could have been included in the study, especially T1rho, which has been suggested as a good parameter in the evaluation of cartilage.[3,40,41] However, due to logistic reasons, MR-imaging time for the specimens was restricted and measuring additional parameters was not possible. In PLM, the lack of true anisotropy might have caused biased results when comparing MRI to anisotropy, since the anisotropy was calculated from the fiber angle images using image entropy.

This study showed that evaluation of the degradative state of articular cartilage using qMRI is improved when using PLSR-

modelling instead of direct correlations. Based on the present findings, PTOA processes change QSM-contrast in cartilage; while the exact reason remains unknown, the collagen fiber network structure appears to change as well, a finding that has been previously linked to changes in QSM contrast.[15,16] Moreover, T2* relaxation time was shown to be a more useful parameter than QSM in the evaluation of cartilage degeneration. Combining the results from both modalities resulted in slightly higher correlations between the measured and PLSR-predicted reference parameters, suggesting that QSM adds to qMRI evaluation of cartilage.

Author contributions

Nykänen: corresponding author, QS- and T2* map calculation, data-analysis, PLM measurements, manuscript drafting and editing.

Sarin: Data analysis, OD measurements, biomechanical measurements, sample preparation, manuscript editing.

Leskinen: MRI ROI definitions, data-analysis, manuscript editing.

Ketola: MRI measurements, manuscript editing.

te Moller: animal experiments, data analysis, biomechanical measurements, manuscript editing.

Tiitu: Histological sample preparation, manuscript editing.

Mancini: animal experiments, design of the study, manuscript editing.

Visser: animal experiments, design of the study, manuscript editing.

Brommer: animal experiments, design of the study, manuscript editing.

van Weeren: animal experiments, design of the study, manuscript editing.

Malda: animal experiments, design of the study, manuscript editing.

Töyräs: design of the study, manuscript editing.

Nissi: design of the study, MRI measurements, data-analysis, manuscript drafting and editing.

All authors: revision for intellectual content, final approval.

Conflict of interest

Authors declare no conflicts of interest.

Funding sources

Academy of Finland, Finnish Cultural Foundation, Northern Savo Regional Fund of Finnish Cultural Foundation, Dutch Arthritis Foundation.

Role of the funding sources

Funding sources had no influence on study design or interpretation.

Acknowledgements

Support from the Academy of Finland (grants #285909, #293970, and #319440), The Northern Savo Regional Fund of the Finnish Cultural Foundation (grant #65161539), the Finnish Cultural Foundation (grant #00180787) and the Dutch Arthritis Foundation, the Netherlands (grants LLP-12 and LLP-22) are gratefully acknowledged. Help from Mr. Abdul Wahed Kajabi in PLM-imaging is gratefully acknowledged.

Supplementary data

Supplementary data to this article can be found online at https://doi.org/10.1016/j.joca.2019.06.009.

References

1. Buckwalter JA, Mankin HK. Instructional Course Lectures, The American Society of Orthopaedic Surgeons – Articular cartilage. Part II: degeneration and osteoarthrosis, repair, regeneration, and transplantation. J Bone Jt Surg 1997;79:612–32.
2. Buckwalter JA, Brown TD. Joint injury, repair, and remodeling: roles in post-traumatic osteoarthritis. Clin Orthop Relat Res 2004;423:7–16.
3. Oei EH, van Tiel J, Robinson WH, Gold GE. Quantitative radiologic imaging techniques for articular cartilage composition: toward early diagnosis and development of disease-modifying therapeutics for osteoarthritis. Arthritis Care Res 2014;66(8):1129–41.
4. Li X, Majumdar S. Quantitative MRI of articular cartilage and its clinical applications. J Magn Reson Imaging 2013;38(5):991–1008.
5. Menashe L, Hirko K, Losina E, Kloppenburg M, Zhang W, Li L, *et al*. The diagnostic performance of MRI in osteoarthritis: a systematic review and meta-analysis. Osteoarthritis Cartilage 2012;20(1):13–21.
6. Schreiner MM, Zbýň Š, Schmitt B, Weber M, Domayer S, Windhager R, *et al*. Reproducibility and regional variations of an improved gagCEST protocol for the in vivo evaluation of knee cartilage at 7 T. Magn Reson Mater Phys Biol Med 2016;29(3):513–21.
7. Zbýň Š, Mlynárik V, Juras V, Szomolanyi P, Trattnig S. Evaluation of cartilage repair and osteoarthritis with sodium MRI. NMR Biomed 2016;29(2):206–15.
8. de Rochefort L, Brown R, Prince MR, Wang Y. Quantitative MR susceptibility mapping using piece-wise constant regularized inversion of the magnetic field. Magn Reson Med 2008;60(4):1003–9.
9. Schweser F, Deistung A, Reichenbach JR. Foundations of MRI phase imaging and processing for quantitative susceptibility mapping (QSM). Z Med Phys 2015;26(1):6–34.
10. Marques J, Bowtell R. Application of a Fourier-based method for rapid calculation of field inhomogeneity due to spatial variation of magnetic susceptibility. Concepts Magn Reson Part B Magn Reson Eng 2005;25(1):65–78.
11. Langkammer C, Liu T, Khalil M, Enzinger C, Jehna M, Fuchs S, *et al*. Quantitative susceptibility mapping in multiple sclerosis. Radiology 2013;267(2):551–9.
12. Goldring MB, Goldring SR. Articular cartilage and subchondral bone in the pathogenesis of osteoarthritis. Ann N Y Acad Sci 2010;1192:230–7.
13. Ea HK, Nguyen C, Bazin D, Bianchi A, Guicheux J, Reboul P, *et al*. Articular cartilage calcification in osteoarthritis: insights into crystal-induced stress. Arthritis Rheumatol 2011;63(1):10–8.
14. Wei H, Dibb R, Decker K, Wang N, Zhang Y, Zong X, *et al*. Investigating magnetic susceptibility of human knee joint at 7 Tesla. Magn Reson Med 2017;78(5):1933–43.
15. Wei H, Gibbs E, Zhao P, Wang N, Cofer GP, Zhang Y, *et al*. Susceptibility tensor imaging and tractography of collagen fibrils in the articular cartilage. Magn Reson Med 2017;78(5):1683–90.
16. Nykänen O, Rieppo L, Töyräs J, Kolehmainen V, Saarakkala S, Shmueli K, *et al*. Quantitative susceptibility mapping of articular cartilage: ex vivo findings at multiple orientations and following different degradation treatments. Magn Reson Med 2018;80(6):2702–16.
17. Liu C. Susceptibility tensor imaging. Magn Reson Med 2010;63(6):1471–7.

18. Hänninen N, Rautiainen J, Rieppo L, Saarakkala S, Nissi MJ. Orientation anisotropy of quantitative MRI relaxation parameters in ordered tissue. Sci Rep 2017;7(1):9606.
19. Wei H, Lin H, Qin L, Cao S, Zhang Y, He N, *et al*. Quantitative susceptibility mapping of articular cartilage in patients with osteoarthritis at 3T. J Magn Reson Imaging 2018;49(6):1665–75.
20. Nissi MJ, Toth F, Wang L, Carlson CS, Ellermann JM. Improved visualization of cartilage canals using quantitative susceptibility mapping. PLoS One 2015;10(7), e0132167.
21. Wang L, Nissi MJ, Toth F, Johnson CP, Garwood M, Carlson CS, *et al*. Quantitative susceptibility mapping detects abnormalities in cartilage canals in a goat model of preclinical osteochondritis dissecans. Magn Reson Med 2017;77(3):1276–83.
22. Dymerska B, Bohndorf K, Schennach P, Rauscher A, Trattnig S, Robinson SD. In vivo phase imaging of human epiphyseal cartilage at 7 T. Magn Reson Med 2018;79(4):2149–55.
23. Tóth F, Johnson CP, Mills B, Nissi MJ, Nykänen O, Ellermann J, *et al*. Evaluation of the suitability of miniature pigs as an animal model of juvenile osteochondritis dissecans. J Orthop Res 2019, https://doi.org/10.1002/jor.24353.
24. Nieminen MT, Rieppo J, Töyräs J, Hakumäki JM, Silvennoinen J, Hyttinen MM, *et al*. T2 relaxation reveals spatial collagen architecture in articular cartilage: a comparative quantitative MRI and polarized light microscopic study. Magn Reson Med 2001;46(3):487–93.
25. Sarin JK, te Moller NC, Mancini IA, Brommer H, Visser J, Malda J, *et al*. Arthroscopic near infrared spectroscopy enables simultaneous quantitative evaluation of articular cartilage and subchondral bone in vivo. Sci Rep 2018;8(1):13409.
26. Bekkers JE, Tsuchida AI, van Rijen MH, Vonk LA, Dhert WJ, Creemers LB, *et al*. Single-stage cell-based cartilage regeneration using a combination of chondrons and mesenchymal stromal cells: comparison with microfracture. Am J Sports Med 2013;41(9):2158–66.
27. Delaine-Smith R, Burney S, Balkwill F, Knight M. Experimental validation of a flat punch indentation methodology calibrated against unconfined compression tests for determination of soft tissue biomechanics. J Mech Behav Biomed Mater 2016;60:401–15.
28. Kiviranta I, Jurvelin J, Säämänen A-M, Helminen H. Microspectrophotometric quantitation of glycosaminoglycans in articular cartilage sections stained with Safranin O. Histochem Cell Biol 1985;82(3):249–55.
29. Rieppo J, Hallikainen J, Jurvelin JS, Kiviranta I, Helminen HJ, Hyttinen MM. Practical considerations in the use of polarized light microscopy in the analysis of the collagen network in articular cartilage. Microsc Res Tech 2008;71(4):279–87.
30. Liu T, Wisnieff C, Lou M, Chen W, Spincemaille P, Wang Y. Nonlinear formulation of the magnetic field to source relationship for robust quantitative susceptibility mapping. Magn Reson Med 2013;69(2):467–76.
31. Schofield MA, Zhu Y. Fast phase unwrapping algorithm for interferometric applications. Optic Lett 2013;28(14):1194–6.
32. Liu Z, Kee Y, Zhou D, Wang Y, Spincemaille P. Preconditioned total field inversion (TFI) method for quantitative susceptibility mapping. Magn Reson Med 2017;78(1):303–15.
33. de Rochefort L, Liu T, Kressler B, Liu J, Spincemaille P, Lebon V, *et al*. Quantitative susceptibility map reconstruction from MR phase data using bayesian regularization: validation and application to brain imaging. Magn Reson Med 2010;63(1):194–206.
34. Xia Y, Moody JB, Alhadlaq H, Hu J. Imaging the physical and morphological properties of a multi-zone young articular cartilage at microscopic resolution. J Magn Reson Imaging 2003;17(3):365–74.
35. Lammentausta E, Kiviranta P, Nissi M, Laasanen M, Kiviranta I, Nieminen M, *et al*. T2 relaxation time and delayed gadolinium-enhanced MRI of cartilage (dGEMRIC) of human patellar cartilage at 1.5 T and 9.4 T: relationships with tissue mechanical properties. J Orthop Res 2006;24(3):366–74.
36. Rautiainen J, Nissi M, Liimatainen T, Herzog W, Korhonen R, Nieminen M. Adiabatic rotating frame relaxation of MRI reveals early cartilage degeneration in a rabbit model of anterior cruciate ligament transection. Osteoarthritis Cartilage 2014;22(10):1444–52.
37. Wang Y, Liu T. Quantitative susceptibility mapping (QSM): decoding MRI data for a tissue magnetic biomarker. Magn Reson Med 2015;73(1):82–101.
38. Schweser F, Robinson SD, Rochefort L, Li W, Bredies K. An illustrated comparison of processing methods for phase MRI and QSM: removal of background field contributions from sources outside the region of interest. NMR Biomed 2017;30(4):e3604.
39. Langkammer C, Schweser F, Kames C, Li X, Guo L, Milovic C, *et al*. Quantitative susceptibility mapping: report from the 2016 reconstruction challenge. Magn Reson Med 2018;79(3):1661–73.
40. Gold GE, Chen CA, Koo S, Hargreaves BA, Bangerter NK. Recent advances in MRI of articular cartilage. Am J Roentgenol 2009;193(3):628–38.
41. Nieminen MT, Nissi MJ, Mattila L, Kiviranta I. Evaluation of chondral repair using quantitative MRI. J Magn Reson Imaging 2012;36(6):1287–99.